Dosimetric evaluation of hybrid brass/stainless-steel apertures for proton therapy

2014 Phys. Med. Biol. 59 5043

(http://iopscience.iop.org/0031-9155/59/17/5043)

IOP Publishing | Institute of Physics and Engineering in Medicine Physics in Medicine & Biology

Phys. Med. Biol. **59** (2014) 5043–5060 doi:10.1088/0031-9155/59/17/5043

Dosimetric evaluation of hybrid brass/ stainless-steel apertures for proton therapy

Hao Chen, Witold Matysiak, Stella Flampouri, Roelf Slopsema and Zuofeng Li

University of Florida Proton Therapy Institute, Jacksonville, Florida, USA

E-mail: zli@floridaproton.org

Received 4 December 2013, revised 11 July 2014
Accepted for publication 16 July 2014
Published 13 August 2014

Abstract

In passive scattering proton therapy, patient specific collimators (apertures) are used to laterally shape the proton beam, and compensators are employed to distally conform proton dose to the target. Brass is a commonly used material for apertures and recently a hybrid brass/stainless-steel (BR/SST) aperture design has been introduced to reduce treatment cost without clinical flow change. We measured stopping power and leakage dose for apertures made of stainless steel and brass in the Proton Therapy system. The linear stopping power ratios for stainless steel (type 304) and brass to water were calculated to be 5.46 and 5.51, respectively. Measured stopping power ratios of SST and BR were 5.51 ± 0.04 and 5.56 ± 0.08, respectively, which agrees with the calculated values within 1%. Leakage dose on the downstream surface of two slabs of Ø18 cm stainless steel apertures (total thickness of 6.5 cm) for the maximum available proton energy (235 MeV) was 1.283% ± 0.004% of the prescription dose, and was smaller compared to the 1.358% ± 0.005% leakage dose measured for existing brass apertures of identical physical dimensions. Therefore, the existing beam range limits for brass aperture slabs used at our institution with safety margin allowances for material composition and delivered beam range uncertainties can be safely applied for the new BR/SST aperture design. Potential range differences in the brass and stainless steel interface regions of the hybrid design were further investigated using EBT3 GafChromic film. Film dosimetry revealed no discernible range variations across the brass and stainless steel interface regions. Neutron dose to the patient from brass and stainless steel apertures was simulated using the Monte Carlo method. The results indicate that stainless steel produces similar patient neutron dose compared to brass. Material activation dose rates of stainless steel were measured over a period of 7 d after irradiation. The measurements showed that the proton induced SST activity is initially lower and also decays at a faster rate than that induced in brass, therefore requires no changes in radiation protection requirements on material disposals. The Monte Carlo

simulation confirmed higher initial activity of brass than stainless steel shortly after irradiation. The hybrid BR/SST aperture design is suitable for clinical use to replace the current brass apertures for all clinically used proton ranges. The existing aperture disposal procedures also satisfy radiation protection requirements for the new hybrid type apertures.

Keywords: proton therapy, double scattering delivery mode, patient specific hardware, monte carlo simulations

(Some figures may appear in colour only in the online journal)

1. Introduction

There is a total of 49 hospital-based proton therapy facilities in operation worldwide as of June 2014 (PTCOG: Particle Therapy Co-Operative Group, http://ptcog.web.psi.ch/) and a total of 105 743 patients had been treated by proton radiation therapy as of the end of 2013 (Statistics of patients treated in hadron therapy centers worldwide 2014) since the first hospital-based proton facility started operation at Loma Linda University Medical Center (LLUMC) in California in 1990 (Slater *et al* 1992). The majority of patients have been treated in the passive scattering mode that is a proton beam delivery technique in which scattering materials spread the beam to the required field size, and range-shifting materials conform it to the distal part of the planning tumor volume (Kanai *et al* 1983).

University of Florida Proton Therapy Institute (UFPTI) has commissioned the IBA (Ion Beam Applications, Louvain-La-Neuve, Belgium) system with cyclotron accelerator and three gantries equipped with the universal nozzle for proton therapy (Paganetti *et al* 2004). The universal nozzles are capable of delivering the beam in double-scattering, single-scattering, uniform-scanning, and pencil beam-scanning modes. The majority of proton patient treatments at UFPTI are being delivered in the double-scattering mode (Slopsema 2012). The IBA nozzle employs a rotating range modulator (RM) wheel synchronized with beam current modulation to obtain a uniform Spread-Out Bragg Peak (SOBP) (Kooy and Lu 2006). The IBA nozzle also uses two contoured scatterers to spread the proton beam from the initial Gaussian profile of a few centimeters to a maximum uniform field size of 24 cm in diameter for a span of clinical ranges in water from 4.6 g cm^{-2} to 23.9 g cm^{-2}. When a uniform field size of 14 cm in diameter or less is requested, the available range increases to a maximum of 28.4 g cm^{-2} in water (Slopsema 2012). An adjustable SOBP modulation width is achieved by synchronizing the rotation of the RM wheel with beam current modulation. An aperture is used in double scattering proton therapy to shape the proton dose to the target laterally and the role of a range compensator is to conform the proton dose to the distal end of the target. Although the multileaf collimator (MLC) is a standard device to laterally shape the dose to the target in photon therapy, it is not commonly used in proton therapy for this purpose.

The universal treatment nozzle installed at UFPTI can be fitted with three sizes of treatment snouts depending on the required irradiated field size. In the smallest snout, only one aperture slab of 12 cm diameter and 6.5 cm thickness can be installed. The medium size snout is equipped with two drawers, each fitting a 18 cm diameter and 3.25 cm thick aperture, yielding 6.5 cm for the total thickness of the stopping material. The biggest snout used in passive scattering uses 25 cm diameter apertures. In order to ease the handling of the large size apertures by therapists, the snout has drawers for maximum three thinner apertures, each having the thickness of 2.16 cm. The required minimum total thickness of the apertures for a given treatment field is determined by the requested proton range plus the distal fall-off and a safety margin, which accommodates

the proton range uncertainty and variability in brass density. An arbitrary value of 2 cm WET (water equivalent thickness) has been added as the additional safety margin allowance.

1.1. Motivation for the study

In the existing clinical flow at UFPTI, the patient specific brass apertures are manufactured by an external company and delivered to the site to undergo the quality assurance procedure prior the treatment. After the treatment, the apertures are moved to a designated storage area where they remain until their measured activity cannot be distinguished from background, before they can be safely disposed of. The material price in manufacturing the apertures is considerable, therefore the institution is actively looking for alternative designs to reduce the cost without modifying the existing clinical flow. One possible solution is to introduce a hybrid design by further dividing the aperture into a single-use patient specific part and a more universal re-usable component.

The selection of the snout size that will be used to deliver the treatment fraction to the patient is determined by the largest field size, and hence the aperture size, due to the fact that the snout change operation requires removing the patient from the treatment table. As a result, some fields in the fraction that could be delivered using a smaller snout must use the current, larger snout because the same outer diameter aperture must be used consistently to deliver all fields in the fraction. In such cases, the aperture material is often not utilized optimally.

The outer ring of the hybrid aperture is made re-usable and may be conceptually viewed as a means of finer adjustment of the snout size, with the exception that the hybrid aperture will be assembled by the quality assurance team and delivered prior to the treatment, thus requiring no further action from the therapists or the technical personnel.

If a proton therapy center relies on an external supplier to provide the patient specific apertures, the shipping costs associated with the hybrid type apertures are lower, since the outer rings are stored on site.

The inner aperture core material remains brass, which has excellent machining properties; however, the outer ring may be made from a less expensive material. The requirement for machinability of the outer ring material becomes also less strict as long as it meets the dosimetric criteria.

2. Materials

2.1. Material selection criteria

The primary considerations in selecting the proton beam field-shaping device are: stopping power, leakage dose, penumbra and conformity, neutron production, residual activation, and cost. Brass and Cerrobend™ are two alloys commonly used for aperture materials, and tungsten is a common material used for MLCs. Cerrobend™ can be conveniently machined but molding and final disposal is complicated due to lead and cadmium contents. Brass apertures, on the other hand, are commonly used in passive scattering proton beam delivery because brass is readily available and easy to machine. Both materials have also comparable stopping powers for protons. The composition of brass varies, but it is commonly made of 62% copper, 35% zinc, and 3% lead. However, the material cost of brass aperture is higher than Cerrobend™.

Larger linear stopping power of high-Z materials stops protons with smaller physical thickness. Based on the tabulated stopping power data (PStar: Physical Measurement Laboratory, NIST) the thickness of brass, cerrobend, and tungsten required to fully

stop 235 MeV protons is 6.5 cm, 7.5 cm and 4.0 cm, respectively (Brenner *et al* 2009). Although the leakage through 8.2 cm tungsten (1.2 mGy Gy^{-1}) is close to that through 6.5 cm brass (1.8 mGy Gy^{-1}) (Klein 2009), tungsten creates more secondary neutrons and x-rays than brass.

The major source of scattered protons comes from the tracks that hit the aperture surface, scatter in the aperture material, and leave through the side wall of the aperture opening rather than coming to full stop in the aperture material (van Luijk *et al* 2001). Geometrically, the penumbra of a proton beam in air linearly depends on the distance between the field shaping device and the patient (Urie *et al* 1986) with the proportionality constant depending on the design of the field shaping device and the depth of interest in the patient. Proton dose profiles shaped using a tungsten MLC have similar scattering profiles compared with that shaped with the divergent brass aperture (Kirk *et al* 2010). Daartz *et al* (2009) at the Massachusetts General Hospital (MGH) reported that the lateral fall-off of a proton beam with the mini-multileaf collimator (MMLC) is generally broader and proton beam range varies from 0.2 mm to 1.2 mm comparing with the brass aperture. For a new field shaping device, the variation of the lateral profile, as well as potential proton range variations, should be evaluated before the device can be used clinically (Engelsman *et al* 2009).

Neutron production and radiation dose due to material activation in passive elements of the nozzle are associated with secondary cancer risk for patients and staff. The patient specific collimator is a major neutron generating element in the double-scattering proton beam delivery (Pérez-Andújar *et al* 2009). For that reason, neutron production as well as residual activation should be an important consideration for a new field-shaping device. According to the measurement by Daartz *et al* (2009), a mini-multileaf collimator produced a neutron dose at the isocenter of 0.03–0.13 mSv Gy^{-1}, which is approximately 1.5–1.8 times smaller than the neutron dose from brass apertures (0.04–0.23 mSv Gy^{-1}). As reported in the literature, the aperture-produced neutron doses from iron and nickel, which are the two major components of stainless steel, are smaller than those from zinc and copper, which are the main constituents of brass (Brenner *et al* 2009). The energies of the secondary neutrons in proton therapy span from the thermal up to the maximum proton energy, although the majority of the neutrons have energies below 10 MeV (Paganetti 2012). Due to difficulties in neutron dosimetry in the mixed proton therapy field, Monte Carlo (MC) simulations are commonly used to evaluate neutron dose inside patients/phantoms (Jiang *et al* 2005, Zheng *et al* 2008).

Patient specific apertures become radioactive when subjected to high energy protons therefore radiation exposures to staff resulting from activation of radiation therapy equipment are subject to regulatory limits and should be routinely monitored. Residual activity of the aperture should decay to the level comparable with natural background before the aperture can be disposed of or re-used. According to cross section measurement for proton-induced reactions (Pearlstein 1989, Sisterson and Vincent 2006), proton-induced residual activation of stainless steel should be of the same order or smaller than that of brass. In a similar study, Cesana *et al* (2010) investigated activity induced in aperture made of bronze and compared measured activities with those predicated by the FLUKA code. In this work we compare the residual radioactivity induced by energetic protons in the currently used brass apertures with the activity in the candidate material (stainless steel).

2.2. Hybrid brass/stainless steel apertures

Based on the material cost, availability, and machining properties, stainless steel has been designated as a material that may be optimal for the new hybrid apertures. Stainless steel

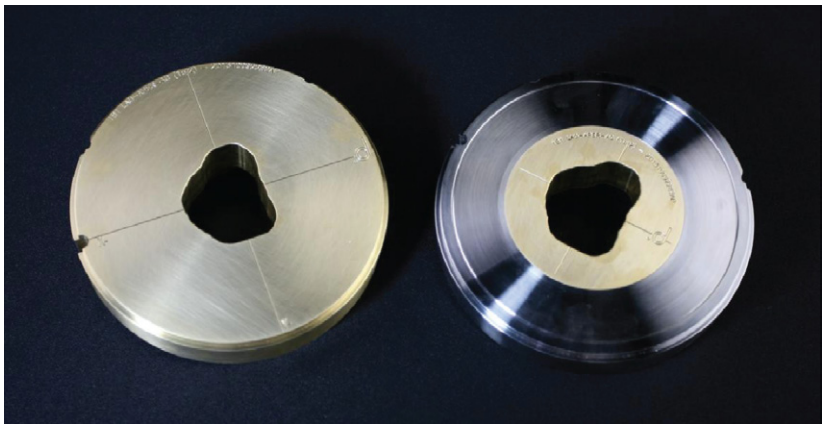

Figure 1. Ø18 cm patient specific apertures: brass (left) and hybrid brass/stainless steel (right)

density (7.48~8.00 g cm^{-3}) is close to that of brass (8.40~8.70 g cm^{-3}) but stainless steel is also less expensive than brass. One pound of brass alloy (C210) costs $3.429 while one pound of stainless steel 304 costs $1.750 as of May 2013 (www.metalprices.com). As a scrap metal, brass recycling price (~$1.75 per lb) is four times that of stainless steel recycling price (~$0.41 per lb). However, the poor machining properties of SST increase the manufacturing cost. A hybrid design is introduced to minimize the combined cost of material and manufacturing. The hybrid BR/SST aperture is composed of a reusable external stainless steel ring combined with a small internal brass core (figure 1). The hybrid aperture in the figure fits the Ø18 cm treatment snout and has a Ø11.43 cm brass core, although diameters of the BR core can be customized to user specifications. The material and manufacturing cost of the external stainless steel ring becomes economically feasible when the device can be re-used. In addition, the amount of brass used for each patient treatment is reduced due to smaller internal brass aperture size.

The proton beam delivery system snout is designed to completely stop the proton beam with BR apertures, and needs to provide the same capability when stainless steel apertures are used. The thickness required to stop 235 MeV protons is 65 mm for brass and 63 mm for iron, which is the major constituent of stainless steel. Stopping power of the stainless steel ring should also be fully evaluated to ensure that the hybrid aperture completely stops the proton beam outside the treatment field portal opening with sufficient safety margins. Protons scattered from edges of the patient specific aperture should be also taken into account for accurate dose-per-monitor-unit calculations, particularly for small field sizes and deep depths (Titt *et al* 2008). In principle, the hybrid aperture should not affect the lateral penumbra because the internal core is still brass, but the external stainless steel ring may introduce alteration of the proton beam profile particularly in the interface regions of brass and stainless steel (Paganetti 2012). Potential change in proton range in the patient with stainless steel compared to brass aperture should also be investigated.

This paper presents the dosimetric evaluation of a new design for passive scattering proton therapy field shaping: a hybrid BR/SST aperture, which has been developed by.decimal, Inc (Sanford, FL, USA). We will evaluate whether the hybrid BR/SST aperture design is suitable for clinical use to replace existing brass apertures.

3. Methods

3.1. Safety margins in maximum beam ranges for the SST only aperture

As discussed earlier, the safety margins adopted by UFPTI which define the maximum proton range that can be used with a given set of apertures, have been calculated conservatively. In addition to the possible variations in proton range and material density, an arbitrary 2 cm WET allowance has been applied. The study of the safety margins with the SST aperture was designed to make sure that the new material does not cause significant reduction of the safety margins and that the level of patient protection is still adequate. First, the stopping power of SST was calculated and measured, and next the safety margins for the existing and the new apertures were experimentally determined for a few selected configurations.

For the calculation of stopping power, the nominal chemical composition of stainless steel type 304 (Chemical Compositions of SAE Wrought Stainless Steels, J405_199806, SAE 1998) was used: 18%~20% of chromium, 8%~10.5% of nickel, 1.25%~2% of manganese, and small amounts (<1% for each) of phosphorus, carbon, silicon, and sulfur, with the balance consisting of iron.

The direct comparison of the safety margins provided by both: SST and BR aperture blocks, was carried out by simultaneous irradiation of the slabs positioned side-by-side in the uniform proton field and measuring the transmitted proton dose as a function of the pre-absorber thickness. Plane-parallel ionization chambers, PPC05, (IBA Dosimetry, Bartlett, TN) were attached to the downstream faces of both aperture slabs and a third plane-parallel ionization chamber was located directly in the proton field to serve as a reference. A proton field of water equivalent range (WER) higher than the expected WET of the investigated aperture set was requested and the transmitted dose was measured. Varying thicknesses of the pre-absorber (solid water slabs) were stacked on the upstream face of both aperture slabs to gradually pull back the proton field range incident on the aperture. The measurements were conducted for the following configurations of the apertures: one slab of Ø18 cm, one slab of Ø25 cm, and two slabs of Ø25 cm.

3.2. Beam profile study of the hybrid BR/SST aperture

Gafchromic EBT3 film (International Specialty Products, Wayne, NJ) was used to investigate the potential impact of the brass-stainless steel interface on the proton beam range in water as well as on the uniformity of lateral dose profiles. The EBT3 film can be used to measure dose up to 10 Gy in the red color channel and 10~40 Gy in the green color channel (Andrés *et al* 2010). The EBT3 film response has been reported to be relatively independent of radiation type and energy (Arjomandy *et al* 2010, Reinhardt *et al* 2012). The film was sandwiched between two layers of the solid water phantoms (single layer thickness of 10 cm) and aligned to the upstream face of the phantom which was located at the central axis (CAX). The gantry was set at 270° and proton beam with the range of 21 cm and SOBP modulation width of 10 cm was blocked by one solid Ø18 cm hybrid BR/SST block with an arbitrarily chosen value of 10.50 cm brass core before reaching the edge of the EBT3 film. Figure 2 shows the setup used in this experiment. After exposure, the EBT3 film was scanned with EPSON EXPRESSION 10000XL scanner and the images were processed with the commercial software FilmQA™ Pro which uses multichannel film dosimetry to produce more consistent results than the traditional single channel method (Micke *et al* 2011).

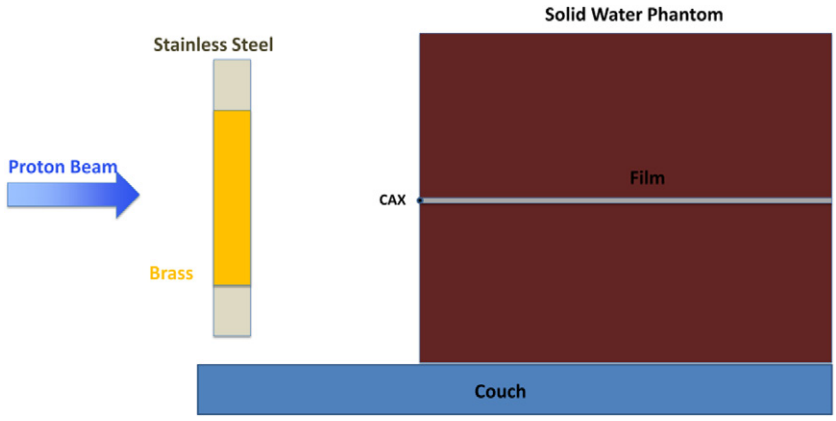

Figure 2. Experimental setup used to investigate potential range differences in the brass and stainless steel interface region with Gafchromic EBT3 film.

3.3. Monte carlo simulation of the secondary neutron dose

The energy spectrum of neutrons produced in proton therapy spans from the thermal to the energy of the incident protons. Because of this, more than a single spectroscopic instrument is required in order to cover the entire range of the neutron energies, which makes neutron spectroscopy in this field challenging (Knoll 2000). Dosimetry of secondary neutrons produced in proton therapy also faces difficulties mostly due to the fact that the radiation field is composed of several types of radiations and separating the neutron component from the mixed field poses a considerable challenge (Wissmann *et al* 2004). Moreover, results of analytical calculations of neutron yield from protons in proton therapy energy ranges may not be reliable due to the lack of evaluated cross-sections for many isotopes used in this study. Owing to the aforementioned difficulties, we resorted to the Monte Carlo method to estimate neutron production in the aperture materials and dose deposition due to neutrons in patient phantom (Agosteo *et al* 1998).

Among the Monte Carlo tools available for this task, the FLUKA code has a track record of reliability in this energy region (Robert *et al* 2013). In this study we used version 2011.1 which was the most up to date version available at the time. The default settings for hadron therapy (the HADRONTHE keyword in the configuration input file) were used in the code to optimize particle tracking conditions. In addition, the threshold for electromagnetic processes was set at 1 GeV which effectively disabled gamma-ray, electron, and positron transport thereby making more efficient use of the processor without significantly affecting the dose distribution in the phantom (Verhaegen and Palmans 2001). Fifty million particle histories were started to achieve the statistical precision better than 4% (±1 standard deviation) in simulated neutron doses in the phantom. The MCNPX code (ver. 2.7) (Pelowitz 2011) with default cross-section libraries distributed with the code was also used for comparison with FLUKA, which uses theory driven models benchmarked with experimental data to compute cross-sections (Fasso *et al* 2005). All transportable particles were enabled in the MCNPX code except electrons and photons.

In order to benchmark the candidate materials for the apertures we adopted the simplified geometry presented by Brenner *et al* (2009) (figure 3). The setup consisted of an annulus-shaped proton source with external and internal diameters of 11.3 cm and 5 cm, respectively which emitted monoenergetic protons perpendicularly to its surface. The energy of the source protons was set at 235 MeV which is the maximum achievable in the proton therapy system

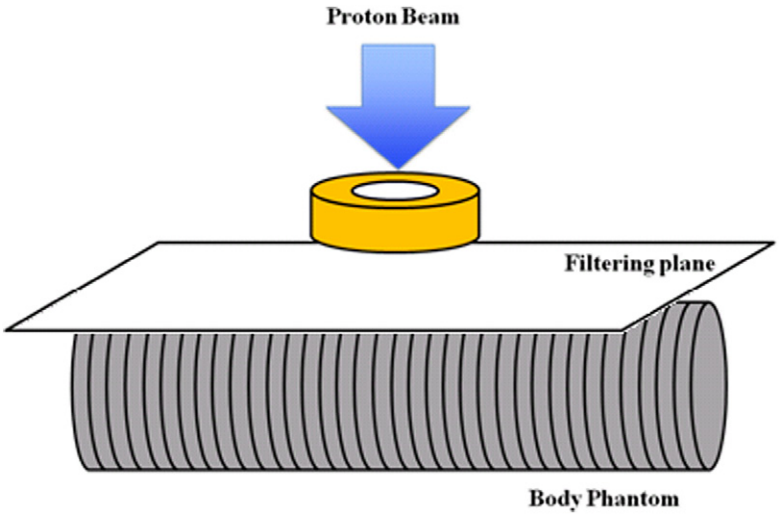

Figure 3. Geometry setup for the Monte Carlo simulation. A uniform mono-energetic 235 MeV proton beam was incident on the aperture face which had circular internal and external diameters of 5 cm and 11.3 cm respectively. Doses due to neutrons originating in the collimator were tallied in 10 mm thick slices along the main axis of a cylindrical homogeneous tissue-equivalent phantom (1.5 m length × 0.5 m diameter) located immediately downstream of the patient-specific collimator.

installed at UFPTI and the one where the highest neutron yield was expected. Positions of the starting particles were uniformly sampled from the source area so that the proton beam was incident on the face of the aperture with inner and outer diameters matching the corresponding dimensions of the source. A cylindrical patient phantom composed of the ICRU soft tissue (ICRU 44) was positioned immediately below the aperture and with the cylinder axis perpendicular to the direction of starting protons. The height of the cylinder was set at 150 cm and the diameter at 50 cm. The phantom cylinder was divided into 150 1 cm thick slices to tally neutron dose as function of lateral distance from the beam.

In order to score only the energy from neutrons produced in the aperture and deposited in the phantom material, a particle filter was employed (figure 3). In the FLUKA code, the filter was implemented as a user routine which assigned zero weight to all particles except neutrons upon entering the filter region, effectively terminating their tracks. In MCNPX the same effect was achieved by assigning zero importance to all particles except neutrons in the filter volume.

In both codes the absorbed dose from neutrons produced in apertures in five selected candidate materials has been tallied. Table 1 presents the dimensions and compositions of the materials used in the Monte Carlo study.

3.4. Leakage dose

The maximum available proton energy of the proton therapy system installed at UFPTI is equivalent to 32 g cm^{-2}. The system snout is designed to allow use of solid aperture blocks sufficient to completely stop the primary protons of the maximum available energy, and needs to achieve equivalent results when SST apertures are used. However, secondary particles (neutrons, photons, secondary protons, and other charged particles) are still present past the aperture. The dose delivered by these particles, which has been termed the "leakage

Table 1. Material compositions and thicknesses used in Monte Carlo simulations.

Material name	Density ($g\,cm^{-3}$)	Thickness (cm)	Composition by mass used for Monte Carlo simulation	Remarks
Brass	8.5	6.5	Copper (62%), Zinc (35%), Lead (3%)	Thickness matches size of currently used apertures
Iron	7.9	6.3		Thickness sufficient to stop 235 MeV protons
Stainless steel	8.0	6.5	Chromium (18%), Iron (74%), Nickel (8%)	″
HD Polyethylene	1.6	19.5	Carbon (84.9%), Hydrogen (14.2%) Boron (0.9%)	″
Tungsten alloy	16.9	4	Tungsten (90%) Nickel (6%) Copper (4%)	″

dose" in the literature (Moyers 2007), was measured in order to see if its magnitude has changed for the new aperture design comparing with the traditional BR apertures. For this purpose a uniform scanning proton field with a maximum available range of $32\,g\,cm^{-2}$ and SOBP modulation width of $5\,g\,cm^{-2}$ was blocked by two Ø18 cm solid BR or SST apertures with the total thickness of 6.5 cm. As in the previous experiment, a PPC05 detector was attached to the distal surface of the downstream aperture. In addition, the leakage dose was measured at the distances of 5 cm, 10 cm, and 20 cm from the downstream surface of the aperture along the CAX. The leakage current of the chamber and electrometer system was measured before the irradiation and subsequently used to correct chamber readings. The measured dose was compared with the known prescription dose (377.3 cGy) and reported as a fraction thereof.

In parallel with the experiment, a Monte Carlo simulation of the leakage dose with FLUKA was performed for both aperture materials: BR and SST. The simulated geometry model consisted of a disc-shaped proton source located immediately upstream of the aperture, and a PPC05 detector, whose material composition and dimensions were built according to the manufacturer's specification. Four separate runs per aperture type (one run per a single detector position) were needed to tally the leakage dose at the locations corresponding to those measured experimentally. In addition, a reference run was required to tally the dose with the apertures removed from the beam path.

3.5. Residual activity of the hybrid BR/SST aperture

Energetic protons interact with the nuclei of the elements constituting brass and stainless steel, and some of these interactions lead to the production of unstable isotopes. According to the measured cross section for proton-induced reactions (Pearlstein 1989, Sisterson and Vincent 2006, Brenner *et al* 2009), the residual activity of stainless steel apertures is characterized by shorter decay times due to shorter half-lives of the involved reaction products. In order to investigate and compare the residual activities induced in brass and stainless steel, two Ø18 cm solid brass apertures and two Ø18 cm solid stainless steel apertures were inserted in the snout of the treatment nozzle in order to block the proton beam, and irradiated with the same nominal proton field (9.1 Gy dose). The proton-induced residual activity was later monitored with a hand-held Geiger-Mueller counter. The FLUKA code was also employed to identify major radionuclides induced in both aperture types with nominal compositions of the alloys. The simulation environment consisted of the apertures and the disc-shaped proton source as in the previous section.

4. Results and discussion

4.1. Safety margin in maximum beam ranges of stainless steel apertures

Safety margins for both SST and BR aperture blocks were evaluated experimentally and results are shown in figures 4(*a*)–(*c*). According to the shape of the measured dose curve, one Ø18 cm brass aperture (thickness of 3.25 cm) is equivalent to 18.3 cm of water. Based on the criteria discussed earlier in the text, the calculated maximum allowed range adopted by our institution for this aperture is 14.1 cm, which provides a safety margin of 4.2 cm. On the other hand, one stainless steel block of the same dimensions is equivalent to 17.8 cm of water, a reduction of 5 mm comparing with brass. As a consequence, the safety margin is also reduced from 4.2 cm to 3.7 cm. Table 2 shows the summary of measurement results for all three configurations of the apertures and compares them with the limits adopted by our institution. The most significant reduction of the safety margin has been observed for two Ø25 cm apertures; however, the measured safety margin for this set of SST apertures is 3.6 cm, which is considered adequate.

The linear stopping power ratios for stainless steel and brass to water were calculated to be 5.46 and 5.51, respectively. The measured stopping power ratios were 5.51 ± 0.04 and 5.56 ± 0.08, respectively, which agree with the calculated values within 1%. The stopping power of stainless steel is only 0.7% lower than brass.

Based on the calculations and the measurements, we conclude that the hybrid BR/SST aperture design can be used to replace existing brass apertures for all available proton ranges without significantly affecting minimum safety margins.

4.2. Depth dose and lateral beam profiles with the hybrid BR/SST aperture

Figure 5 shows the dose map of an arbitrary 10 cm depth × 25.2 cm inline field taken with the EBT3 film and processed with the FilmQA™ Pro software. The dose distribution shown in the film is more uniform closer to the central axis, and the uniformity decreases with increasing off-axis distance. The figure also shows that the proton beam penetrated deeper in the region corresponding to the stainless steel ring. This can be examined in more detail by extracting profiles from the dose map shown in figure 5. Figure 6 (left) shows SOBP profiles extracted from the dose map at arbitrary five lateral positions: the central axis as well as (2.54, 5.08, 5.84, 7.62) cm from the central axis in the inline plane. After passing through the aperture material, the modulated region at the central axis had a residual length of 2.2 cm, which was consistent with the requested range and modulation width of the combined WET of the aperture and the solid water phantom. Away from the axis, in the region corresponding to the SST ring, the length of the modulated region increased, which can be explained by the lower stopping power of the stainless steel outside ring compared with the brass core. The decrease in absolute dose away from the central axis observed in the relative SOBP profiles can be explained by higher scattering in the high-Z materials of the aperture before entering the solid water/film phantom. Figure 6 (right) shows lateral beam profiles in the inline direction at six arbitrary depths: (1.07, 2.13, 2.56, 2.96, 3.41, 3.84) cm. The deeper profiles clearly show reduced width of the flat region and prominent lateral peaks due to the range difference between brass and stainless steel.

As noted earlier, the diameter of the brass core was chosen to be 10.50 cm. The position of the virtual SAD in the UFPTI system is 230 cm and the snout position (the distance between downstream face of the aperture and the isocenter) in this setup was 20 cm. Based on this geometry description, the projections of the brass and stainless steel interface at the depths of (1.07, 2.13, 2.56, 2.96, 3.41, 3.84) cm were located at radial distances of (5.78, 5.80, 5.81,

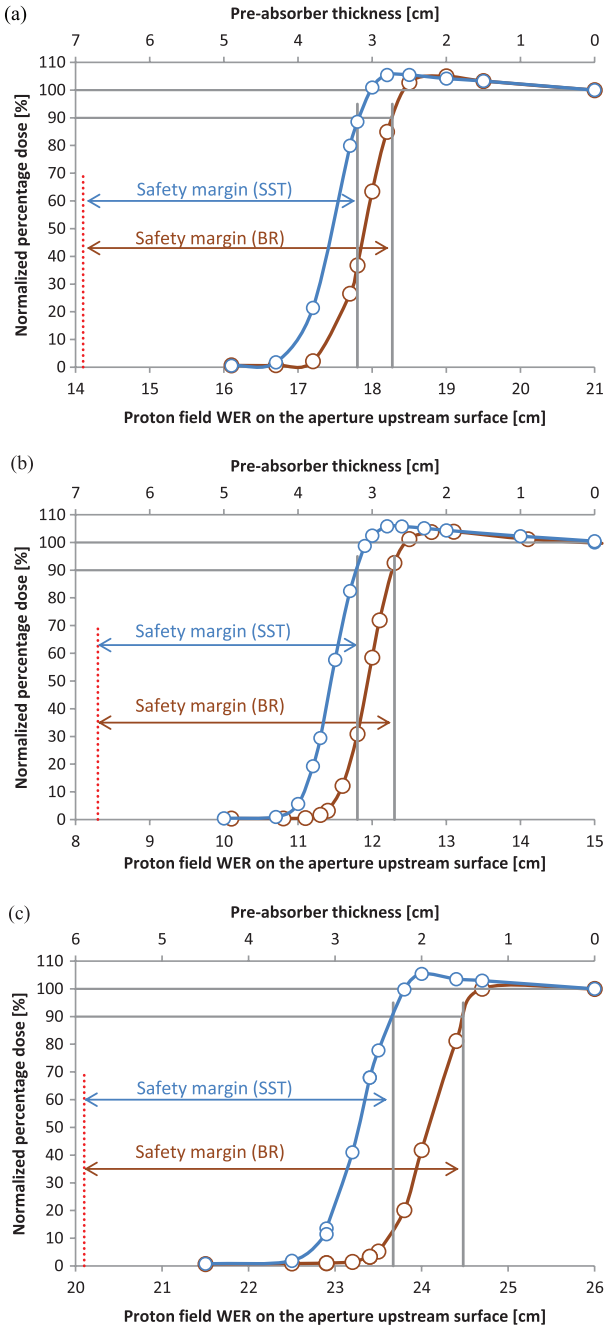

Figure 4. Measured normalized percentage doses after passing (a) one Ø18 cm aperture, (b) one Ø25 cm aperture, and (c) two Ø25 cm stainless steel (blue) and brass (brown) apertures. The top horizontal axis shows the pre-absorber thickness and the bottom axis shows the water equivalent range of the beam entering the aperture. Vertical axis depicts the relative dose measured on the downstream face of the apertures normalized to the maximum dose in the flat SOBP region. The vertical dotted line designates the maximum proton beam range allowed for the given aperture set. Smooth lines have been added to the plots as a guide to the eye.

Table 2. Summary of measured ranges and safety margins provided by BR and SST aperture slabs.

Aperture configuration	Calculated maximum allowed range for this set of aperture blocks (WET cm)	Brass		Stainless steel		Safety margins reduction due to lower stopping power of SST (WET cm)
		Measured range (WET cm)	Safety margin (WET cm)	Measured range (WET cm)	Safety margin (WET cm)	
Ø18 cm × 1	14.1	18.3	4.2	17.8	3.7	0.5
Ø25cm × 1	8.3	12.3	4.0	11.8	3.5	0.4
Ø25cm × 2	20.1	24.5	4.4	23.7	3.6	0.8

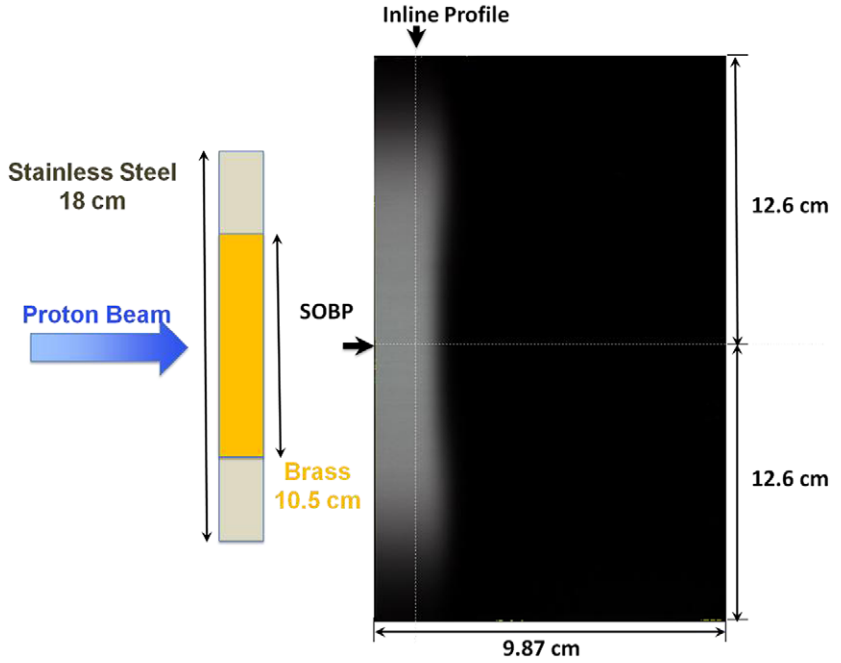

Figure 5. Dose map of an arbitrary 10 cm depth × 25.2 cm inline field taken with the EBT3 film downstream of one brass/stainless steel aperture and processed with the FilmQA™ Pro software. See figure 2 for the experimental setup.

5.82, 5.84, 5.85) cm, respectively, in the inline profile. Figure 6 (right) revealed no discernible distortion of the profiles that would indicate proton range variations across the brass and stainless steel interface regions.

4.3. Secondary neutron dose: simulation results

Figure 7 presents the distribution of neutron doses in phantom from neutrons produced in the aperture as function of the lateral position along the phantom simulated with FLUKA and MCNPX Monte Carlo codes for five candidate aperture materials. Fifty million source protons were started in each simulation which resulted in statistical uncertainty of the results below 4%. Although FLUKA shows absorbed dose values approximately 20% higher than MCNPX, the relative neutron doses for all studied materials are consistent.

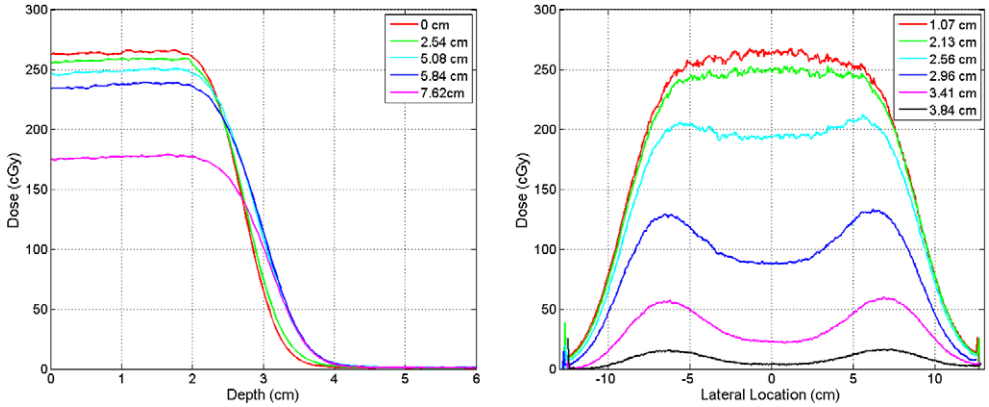

Figure 6. Depth dose profiles in the inline plane at different distances from the central axis (left) and inline profiles at different depths in the phantom (right) extracted from the dose map in figure 5.

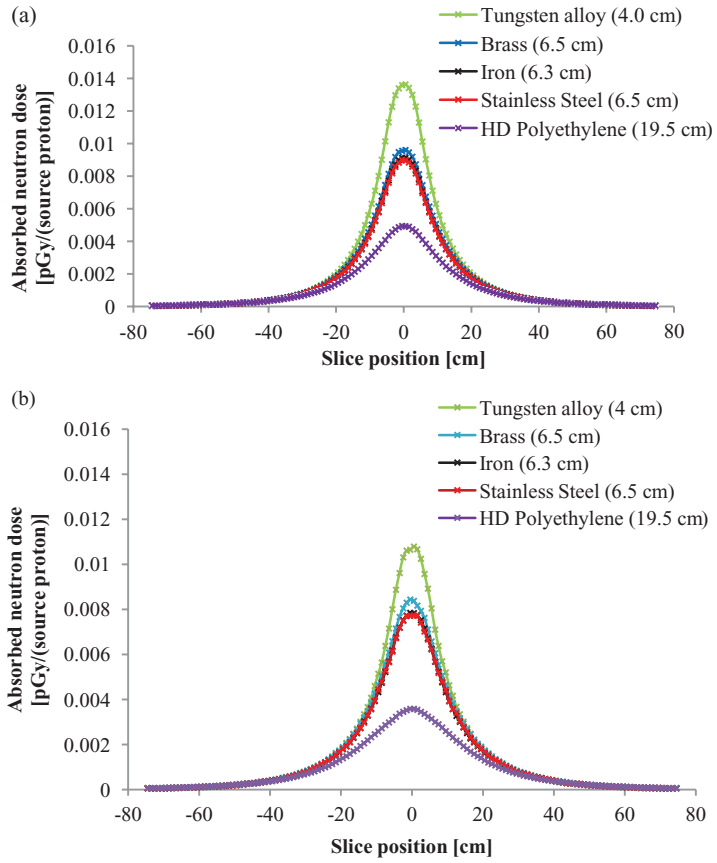

Figure 7. Monte Carlo simulated doses to the phantom from neutrons produced by mono-energetic 235 MeV protons incident on patient-specific collimators made of different materials. Results obtained using FLUKA (*a*) and MCNPX (*b*). See figure 3 caption for geometry description.

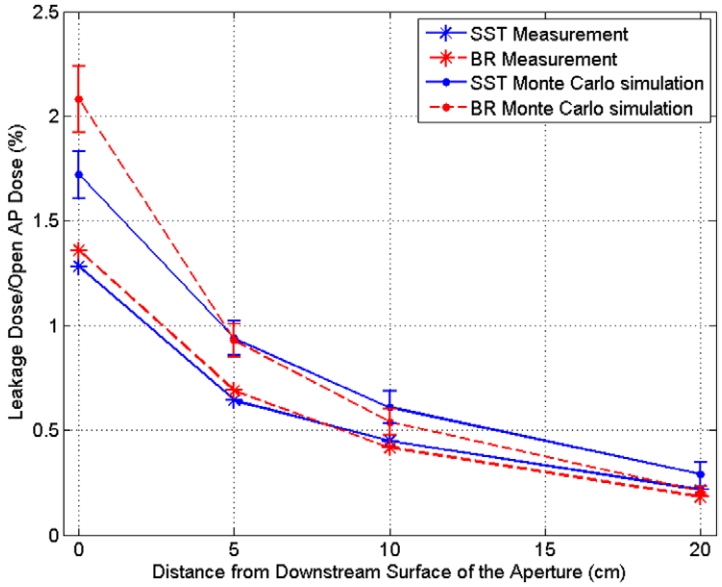

Figure 8. Aperture leakage dose relative to open field dose as function of distance from downstream aperture surface. Measurement (stars) and Monte Carlo simulation (full circles) for both aperture materials: stainless steel (blue) and brass (red).

Table 3. Dose rate measured at the surface of the apertures (mR/hr).

Time	BR_A	BR_B	BR_C	BR_D	SST_A	SST_B	SST_C	SST_D
0	200	200	200	200	115	112	110	35
0:15					70	61	51	21
0:30	75	73	80	30	48	40	40	8
1:00					15.5	15	13	4
1:30	30	30	30	7.8	10	9	7.8	2.5
2:40	7.5	7.5	7.5	3	4.5	4	3.5	1
1D 7:50	1.9	1.9	2.8	1	1.2	1	0.8	0.45
2D 7:50	0.7	0.6	0.6	0.3	0.4	0.4	0.3	0.14
3D 7:50	0.6	0.5	0.45	0.25	0.3	0.25	0.2	0.12
4D 7:50	0.55	0.45	0.4	0.22	0.25	0.2	0.15	0.1
5D 7:50	0.5	0.4	0.35	0.2	0.25	0.2	0.15	0.09
6D 7:50	0.45	0.4	0.35	0.2	0.2	0.16	0.13	0.07

The material with the lowest neutron production is high density polyethylene. However, due to room constraints in the nozzle as well as negative effects on penumbra, HD polyethylene has not been adopted as the aperture material. At the other extreme is tungsten alloy which is characterized by the highest neutron production among the materials examined in this study. Our results confirm the findings of others who studied the suitability of tungsten as the multi leaf collimator material (Moskvin *et al* 2011). Between the two extremes are the remaining three candidate materials, which are characterized by similar neutron doses induced in the phantom.

On the absolute scale our results show neutron doses that are several times lower than those presented by Brenner *et al* (2009). The discrepancy in MCNPX results is due to the fact that the authors of this publication used a different set of cross-sections based on a custom compilation of available experimental data (Brenner, personal communication), whereas in

Table 4. Dose rate measured at a distance of 30 cm from the apertures (mR/hr).

Time	BR_A	BR_B	BR_C	BR_D	SST_A	SST_B	SST_C	SST_D
0	25	30	30	12	10	5	6	2
0:15					4	3.8	2.5	1.4
0:30	40	35	35	9	3	1.7	1.4	0.7
1:00					0.9	0.8	0.7	0.2
1:30	1.1	1	0.9	0.4	0.4	0.4	0.3	0.2
2:40	0.4	0.3	0.35	0.2	0.2	0.2	0.2	0.1
1D 7:50	0.18	0.15	0.3	0.14	0.21	0.2	0.14	0.08
2D 7:50	0.1	0.08	0.09	0.05	0.08	0.08	0.05	0.035
3D 7:50	0.06	0.06	0.05	0.04	0.06	0.045	0.05	0.03
4D 7:50	0.05	0.05	0.04	0.03	0.05	0.045	0.04	0.025
5D 7:50	0.05	0.05	0.05	0.025	0.04	0.03	0.03	0.02
6D 7:50	0.05	0.05	0.05	0.03	0.04	0.03	0.03	0.01

our work the MCNPX code was used with the default ENDF cross-sections. The FLUKA code uses ENDF cross-sections for neutron induced reactions only and the cross-sections for proton induced reactions are theory driven (Tripathi *et al* 1997, Sihver *et al* 2012). The relative convergence of the outcomes obtained with two different approaches gives us more confidence in our results.

4.4. Leakage dose

Figure 8 presents measured and simulated leakage doses as a function of the distance from downstream aperture surface for both aperture materials: brass and stainless steel. The leakage dose measured immediately downstream of two Ø18 cm both types stainless steel and brass apertures was (1.283 ± 0.004)% and (1.358 ± 0.005)% of the prescription dose, respectively. The leakage dose decreased from 1.283% to 0.216% of open aperture dose for SST and from 1.358% to 0.183% of open aperture dose for BR when the distance from downstream surface increase from zero to 20 cm. Monte Carlo simulations with the FLUKA code show the leakage dose which is higher than that measured experimentally. This difference may be in part attributed to the fact that a mono-energetic source of 235 MeV protons was used in the simulation, whereas a modulated field was chosen for the measurement. The simulated leakage dose follows the trend of the experimental measurement, and indicates that there are no significant differences in the leakage dose between brass and stainless steel. According to the figure, absorbed patient dose due to leakage will not exceed 0.5% of the planned dose as long as the air gap between aperture and patient is maintained above 10 cm. Based on the measurements of safety margins in section 4.1 and due to the fact that the leakage doses are not significantly different, the beam range limits of brass aperture slabs used at our institution, with safety margin allowances for material composition and delivered beam range uncertainties, may be applied directly to BR/SST apertures.

4.5. Residual activity of brass and stainless steel

Measurements of brass and stainless steel activation decay characteristics are presented in tables 3 and 4. Two pairs of physical apertures made of BR and SST were studied. Letters A and B denote the upstream and downstream surfaces of aperture slab one, and letters C and D stand for the corresponding surfaces of aperture slab two. As shown in the tables, the residual activity of stainless steel was initially lower than that of brass, therefore requiring no changes in radiation protection requirements on material disposals.

At an arbitrary time of 30 min after irradiation, Monte Carlo simulations also predict higher total brass activity (11.1 mBq/(source particle)) than stainless steel (4.8 mBq/(source particle)), although direct comparison with dose rate measurement cannot be made mostly due to the self shielding effect. Monte Carlo simulation also shows that the total activity of brass at this time is dominated by ^{62}Cu ($T_{1/2}$ = 9.7 min), whereas ^{53}Fe ($T_{1/2}$ = 8.5 min) and ^{52}Mn ($T_{1/2}$ = 21 min) contribute mainly to the activity of stainless steel.

5. Conclusions

The existing design of brass patient specific apertures used in passive delivery proton therapy was compared with the new design of hybrid BR/SST apertures. The results of the experimental study show that even though the SST stopping power is lower than BR so that the safety margins provided by stainless steel have decreased comparing with brass, the new SST still provides sufficient safety margins without any modifications in the TPS up to the maximum proton range of 32 g cm^{-2}. Proton range in water and the shape of the lateral profiles in the region projected by the brass core are not affected by the stainless steel outer ring. The interface of brass and stainless steel does not introduce discernible distortion of the lateral profile. The measured and Monte Carlo simulated leakage doses are of comparable levels for both stainless steel and brass. Furthermore, patient neutron dose, as simulated by FLUKA and MCNPX codes, is lower for stainless steel than brass. Finally, as shown by the measurements and Monte Carlo simulations, radiation risk to the staff due to proton-induced activation of the apertures is slightly reduced with the new design. The initial residual activity in stainless steel is lower than in brass, and also decays at a faster rate, requiring no alteration in the storage of existing apertures. After the cooling off period, the BR/SST apertures are disassembled, so that the brass cores can be disposed of and the SST shells reused.

We conclude that the hybrid BR/SST aperture design is suitable for clinical use to replace the current brass apertures for all clinically used proton ranges without any modifications in the existing clinical flow.

Acknowledgments

This project was partially supported by.decimal, Inc. Photo of the hybrid aperture in figure 1, as well as material composition specifications were provided by Salvatore Gerace, PhD.

References

Agosteo S, Birattari C, Caravaggio M, Silari M and Tosi G 1998 Secondary neutron and photon dose in proton therapy *Radiother. Oncol.* **48** 293–305

Andrés C, del Castillo A, Tortosa R, Alonso D and Barquero R 2010 A comprehensive study of the Gafchromic EBT2 radiochromic film. A comparison with EBT *Med. Phys.* **37** 6271

Arjomandy B, Tailor R, Anand A, Sahoo N, Gillin M, Prado K and Vicic M 2010 Energy dependence and dose response of Gafchromic EBT2 film over a wide range of photon, electron, and proton beam energies *Med. Phys.* **37** 1942–7

Berger M J 1993 Penetration of proton beams through water 1. Depth-dose distribution, spectra and LET distribution *NIST Technical Note* NISTIR 5226

Brenner D J, Elliston C D, Hall E J and Paganetti H 2009 Reduction of the secondary neutron dose in passively scattered proton radiotherapy, using an optimized pre-collimator/collimator *Phys. Med. Biol.* **54** 6065–78

Candela J C, Crispin-Ortuzar M and Aslaninejad M 2011 Depth-dose distribution of proton beams using inelastic-collision cross sections of liquid water *Nucl. Instrum. Methods Phys. Res.* **269** 189–96
Cesana A, Mauro E and Silari M 2010 Induced radioactivity in a patient-specific collimator used in proton therapy *Nucl. Instrum. Methods Phys. Res.* **268** 2272–80
Daartz J, Bangert M, Bussière M R, Engelsman M and Kooy H M 2009 Characterization of a mini-multileaf collimator in a proton beamline *Med. Phys.* **36** 1886–94
Diffenderfer E S, Ainsley C G, Kirk M L, McDonough J E and Maughan R L 2011 Comparison of secondary neutron dose in proton therapy resulting from the use of a tungsten alloy MLC or a brass collimator system *Med. Phys.* **38** 6248–56
Engelsman M, Lu H-M, Herrup D, Bussiere M and Kooy H M 2009 Commissioning a passive-scattering proton therapy nozzle for accurate SOBP delivery *Med. Phys.* **36** 2172
Fasso A, Ferrari A, Ranft J and Sala P R 2005 *FLUKA: a multi-particle transport code* CERN-2005–10 (2005), INFN/TC_05/11, SLAC-R-773
Jiang H, Wang B, Xu X G, Suit H D and Paganetti H 2005 Simulation of organ-specific patient effective dose due to secondary neutrons in proton radiation treatment *Phys. Med. Biol.* **50** 4337
Kanai T, Kawachi K, Matsuzawa H and Inada T 1983 Broad beam three-dimensional irradiation for proton radiotherapy *Med. Phys.* **10** 344
Kirk M, Ainsley C and McDonough J 2010 Comparison of proton MLC with non-divergent brass and tungsten apertures *52th Annual Meeting of the American Association of Physicists in Medicine* (*Philadelphia, July 2010*)
Klein E E 2009 New developments in proton therapy delivery systems *Symp.on the Promises and Perils of Proton Radiotherapy* (*Baltimore, May 2009*)
Knoll G F 2000 *Radiation Detection and Measurement* (New York: Wiley)
Kooy H and Lu H-M 2006 Optimization of current modulation function for proton spread-out Bragg peak fields *Med. Phys.* **33** 1281
McGinley P H 1992 Photoneutron production in the primary barriers of medical accelerator rooms *Health Phys.* **62** 359–62
MetalPrices.com 2013 MetalPrices.com, Inc. Market Data viewed 1 October 2013 (http://metalprices.com)
Micke A, Lewis D F and Yu X 2011 Multichannel film dosimetry with nonuniformity correction *Med. Phys.* **38** 2523
Moskvin V, Cheng C W and Das I J 2011 Pitfalls of tungsten multileaf collimator in proton beam therapy *Med. Phys.* **38** 6395
Paganetti H 2012a Late effects from scattered and secondary radiation *Proton Therapy Physics* ed H Paganetti (Boca Raton, FL: CRC)
Paganetti H 2012b Monte Carlo simulations *Proton Therapy Physics* ed H Paganetti (Boca Raton, FL: CRC)
Paganetti H, Jiang H, Lee S Y and Kooy H M 2004 Accurate Monte Carlo simulations for nozzle design, commissioning and quality assurance for a proton radiation therapy facility *Med. Phys.* **31** 2107
Pearlstein S 1989 Medium-energy nuclear data libraries: a case study, neutron- and proton-induced reactions in 56-Fe *Astrophys. J.* **346** 1049–60
Pelowitz D 2011 MCNPX 2.7.0 extensions LANL, LA-UR-11-02295
Pérez-Andújar A, Newhauser W D and DeLuca P M Jr 2009 Neutron production from beam-modifying devices in a modern double scattering proton therapy beam delivery system *Phys. Med. Biol.* **54** 993–1008
Reinhardt S, Hillbrand M, Wilkens J J and Assmann W 2012 Comparison of Gafchromic EBT2 and EBT3 films for clinical photon and proton beams *Med. Phys.* **39** 5257–62
Robert C *et al* 2013 Distributions of secondary particles in proton and carbon-ion therapy: a comparison between GATE/Geant4 and FLUKA Monte Carlo codes *Phys. Med. Biol.* **58** 2879
Sihver L, Lantz M, Bohlen T T, Mairani A, Cerutti A F and Ferrari A 2012 A comparison of total reaction cross section models used in FLUKA, GEANT4 and PHITS *2012 IEEE Aerospace Conf.* (*Big Sky, Mar. 2012*)
Sisterson J M and Vincent J 2006 Cross section measurements for proton-induced reactions in Fe and Ni producing relatively short-lived radionuclides at E=140–500 MeV *Nucl. Instrum. Methods Phys. Res. Sect. B: Beam Interact. Mater. Atoms* **251** 1–8
Slater J M, Archambeau J O, Miller D W, Notarus M I, Preston W and Slater J D 1992 The proton treatment center at Loma Linda University Medical Center: rationale for and description of its development *Int. J. Radiat. Oncol. Biol. Phys.***22** 383–9

Slopsema R 2012 Beam delivery using passive scttering *Proton Therapy Physics* ed H Paganetti (Boca Raton, FL: CRC)

Smith A *et al* 2009 The M D Anderson proton therapy system *Med. Phys.* **36** 4068

Particle Therapy Cooperative Group (PTCOG) 2014 Statistics of patients treated in hadron therapy centers worldwide viewed 30 June 2014 (http://ptcog.web.psi.ch/patient_statistics.html)

Tayama R, Fujita Y, Tadokoro M, Fujimaki H, Sakae T and Terunuma T 2006 Measurement of neutron dose distribution for a passive scattering nozzle at the Proton Medical Research Center (PMRC) *Nucl. Instrum. Methods Phys. Res. Sect. A* **564** 532–6

Titt U, Zheng Y, Vassiliev O N and Newhauser W D 2008 Monte Carlo investigation of collimator scatter of proton-therapy beams produced using the passive scattering method *Phys. Med. Biol.* **53** 487–502

Tripathi R K, Wilson J W and Cucinotta F A 1997 Accurate universal parameterization of absorption cross sections II— neutron absorption cross sections *Nucl. Instrum. Methods Phys. Res. Sect. B: Beam Interact. Mater. Atoms***129** 11–5

Urie M M, Sisterson J M, Koehler A M, Goitein M and Zoesman J 1986 Proton beam penumbra: effects of separation between patient and beam modifying devices *Med. Phys.* **13** 734

van Luijk P, van 't Veld A A, Zelle H D and Schippers J M 2001 Collimator scatter and 2D dosimetry in small proton beams *Phys. Med. Biol.* **46** 653

Verhaegen F and Palmans H 2001 A systematic Monte Carlo study of secondary electron fluence perturbation in clinical proton beams (70–250 MeV) for cylindrical and spherical ion chambers *Med. Phys.* **28** 2088–95

Wissmann F, Langner F, Roth J and Schrewe U 2004 A mobile TEPC-based system to measure the contributions to H*(10) at flight altitudes *Radiat. Prot. Dosim.***110** 347–9

Zheng Y, Fontenot J, Taddei P, Mirkovic D and Neuhauser W 2008 Monte Carlo simulations of neutron spectral fluence, radiation weighting factor and ambient dose equivalent for a passively scattered proton therapy unit *Phys. Med. Biol.* **53** 187